Kinetic modelling of Polythionic Acids in Wackenroder Reaction

Elvira Spatolisano[a,], Laura A. Pellegrini[a], Lucia Bonoldi[b], Alberto R. de Angelis[b], Daniele G. Moscotti[b], Micaela Nali[b]*

[a]GASP - Group on Advanced Separation Processes & GAS Processing, Dipartimento di Chimica, Materiali e Ingegneria Chimica "G. Natta", Politecnico di Milano, Piazza Leonardo da Vinci 32, 20133 Milano, Italy

[b]Eni S.p.A. Research and Technological Innovation Department, via F. Maritano 6, I-20097 San Donato Milanese, Italy

[*]Corresponding author: Elvira Spatolisano (elvira.spatolisano@polimi.it; phone: +39 02 2399 3207; fax: +39 02 2399 3280)

Abstract

The Wackenroder reaction, which consists in the liquid phase oxidation of H_2S by SO_2 to produce polythionates, is at the base of the HydroClaus process, a novel H_2S valorization technology patented by Eni S.p.A. In this work, polythionate kinetics in Wackenroder reaction is studied. The influence of operating conditions, i.e., temperature and residence time, on the system has been investigated through experimental data collected in a bench scale reactor. The experimental apparatus behaviour has been assessed by means of a step tracer experiment. As the reacting system is a gas-liquid one, the controlling regime has been identified thanks to a qualitative analysis of the available tests. Due to the very complex nature of the reacting system and the large number of chemical species involved, a single and two-lumped models have been considered to describe the phenomenon. Results show good agreement between the experimental data and the developed model.

Keywords: polythionic acids, Wackenroder reaction, gas-liquid reactions, H_2S valorization

Abbreviations

CBA	Cold Bed Adsorption
CSTR	Continuous Stirred Tank Reactor
HDS	HydroDeSulphurization

HCK	HydroCracKing
PFR	Plug Flow Reactor
RTD	Residence Time Distribution
SCOT	Shell Claus Off Gas Treating
SRU	Sulphur Recovery Unit
TGCU	Tail Gas Clean up Unit

1. Introduction

With more stringent fuel regulations and increasing environmental concerns, together with the need to process sourer crude oils and natural gases (De Guido et al., 2018; Pellegrini et al., 2019), sulphur recovery has become one of the leading issues in emissions reduction (Rouquette et al., 2009). Numerous processes are widely used in the refining industry, for the purpose of transformation and/or capture of the sulphur compounds contained in the petroleum fractions (Heinrich and Kasztelan, 2001). Usually, the sulphur species are concentrated and then transformed mainly into hydrogen sulphide (H_2S) in hydrodesulphurization (HDS) units and in hydrocracking or catalytic-cracking (HCK) units, followed by the H_2S capture and enrichment via solvent washing (De Guido et al., 2017) (e.g., amine units), and finally the H_2S conversion into elemental sulphur in the sulphur recovery unit (SRU). The most common method of converting H_2S into elemental sulphur is the Claus process. The Claus process consists in the vapour phase oxidation of hydrogen sulphide to form water and elemental sulphur, according to the two steps:

$$H_2S + 3/2\, O_2 \rightarrow H_2O + SO_2 \quad (1)$$

$$2H_2S + SO_2 \rightarrow 2H_2O + 3/x\, S_x \quad (2)$$

with x variable as a function of temperature.

Depending on the H_2S initial concentration, different process modifications are available. However, regardless of the process configuration selected, the exit stream from the Claus plants usually cannot meet environmental emission requirements, and, consequently, a tail gas clean-up unit (TGCU) is often employed to eliminate the last sulphur compounds. According to the available literature, the most commonly used processes are Shell Claus Offgas Treating (SCOT) (Groenendaal, 1974), SUPERCLAUS (Borsboom et al., 2005), and Cold Bed Adsorption (CBA) (Kunkel et al., 1977).

Although the Claus process offers the advantages of a quite simple configuration and low investment and operating costs for large scale applications and high H_2S inlet contents, when the acid gas stream contains less than 15% mol of H_2S, it may be difficult to operate such facilities. For typical medium scale applications (sulphur production up to approximately 5 long tons per day of sulphur), liquid reduction-oxidation (redox) processes are quite common (Spatolisano et al., 2021a). In this case, the sulphur is produced as an aqueous slurry. As opposite to large scale plants, the middle scale liquid phase redox processes panorama is more variegate. In this respect, research efforts are devoted to develop alternatives for the simultaneous H_2S abatement and valorization.

Among them, Eni S.p.A. (de Angelis et al., 2005) proposed an alternative for the middle scale H_2S valorization processes, that is the HydroClaus process, based on the Wackenroder reaction. According

to the HydroClaus process, hydrogen sulphide is oxidised in liquid phase to polythionate ions through the following reaction:

$$(2n-5)H_2S+(n+5)SO_2 \rightarrow 3S_nO_6^{2-}+6H^++(2n-8)H_2O \quad (3)$$

with typical operating conditions being ambient pressure, ambient temperature and variable pH from 3 to 2. The reactants ratio H_2S/SO_2 strongly affects the type and the distribution of products formed (Spatolisano et al., 2021b). When a significant excess of H_2S is fed to the reactor, sulphur and short chain polythionates are preferentially produced (mainly $S_4O_6^{2-}$). On the other hand, when SO_2 is the most abundant reagent, $S_nO_6^{2-}$, with n ranging from 4 to 8, are the main products (Barbieri and Croatto, 1964; Barbieri and Faraglia, 1962). Also, the pH of the reaction environment is responsible of determining the nature of the products. At increasing pH, the produced sulphur decreases and polythionates become shorter up to the formation of thiosulphate only, at pH > 8 (Barbieri and Croatto, 1964).

As opposed to sulphur, polythionates are significantly valuable products for their extreme flexibility. They can find application in several fields, as in chemical milling of magnesium and its alloys; in cooling for metal machining; in agriculture or in gold leaching processes. Nevertheless, due to their very complex nature and their tendency to rapidly decompose, they were neglected for many years. No kinetic modelling of the Wackenroder reaction is reported in literature, neither its mechanism has been clearly assessed. To overcome these issues, the aim of this work is to propose a preliminary kinetic model for the HydroClaus reacting system, in order to offer a clarification of the observable reacting phenomena. The Central Composite Design has been selected for planning the HydroClaus experimental campaign, considering residence time and temperature as variable factors. The experimental apparatus used was a continuous stirred tank reactor (CSTR), whose behaviour has been assessed thanks to a step tracer experiment. As the reacting system is a gas – liquid one, the controlling regime has been identified through an appropriate analysis of the available experimental data. Once determined both the reactor behaviour and the controlling regime, kinetic parameters have been evaluated through an ad-hoc developed non-linear regression routine, detailed in the following sections.

2. Experimental

The experimental apparatus used for collecting kinetic data is reported in Figure 1.

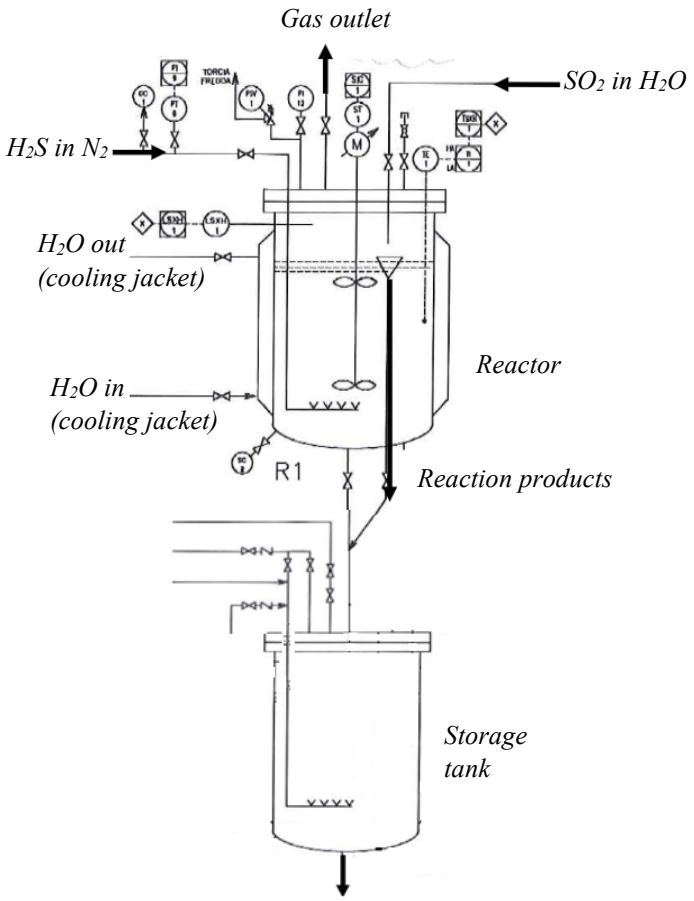

Figure 1. Experimental apparatus for the preparation of the Wackenroder solution (arrows not specified refer to pipeline and instrumentation).

The stainless steel (AISI 316L) reactor, whose volume is V = 2.4 l, is fed with a solution of saturated SO_2 at atmospheric pressure (6 wt.%, $C_{SO_2}^{\ IN} = 0.9647$ mol/L) in water together with a gaseous stream of H_2S in N_2, with flow rates of, respectively, 2 Nl/h and 1 Nl/h. The pH of the reaction environment was stabilized around 2 when starting each test, through a H_2SO_4 aqueous solution, to guarantee constant pH reaction environment during the whole test. The reacting zone is kept under agitation, to ensure good mixing. The reactor pressure is fixed at 3 bara, while the reaction temperature has been varied between 20 and 50°C, to verify its effect on products distribution. The reaction temperature is controlled by means of a cooling water jacket, being the reaction fairly exothermic. The residence time in the reactor (τ) has been varied through the manipulation of the SO_2 solution flow rate, being SO_2 the only liquid phase species fed to the reactor. Once a time $t = 3\tau$ has passed, the product, collected in the storage tank, was sampled to evaluate its composition. The product appears as a yellow milky dispersion, more or less stable and homogeneous depending on the operating conditions selected in the reactor. With aging, the product mixture separates in two phases: one solid, deposited on the bottom of the sample, and one liquid, in which the solid is dispersed. To force the liquid – solid separation, about 2000 ppmw of nitrate-based polyelectrolyte flocculant (EstFloc 175, by Est Chemie Srl) are added to the reaction product. For determining the polythionates

concentration in the solid and aqueous phase fractions, the two phases were weighed and analysed through Raman spectroscopy and High Pressure Liquid Chromatography (HPLC) with UV detector, respectively. Raman spectra were acquired by means of a MicroRaman HORIBA Evolution spectrometer, equipped with 532 nm laser excitation and calibrated at every use with a pure Silicon specimen ($1/\lambda_{max}$ = 520.7 cm^{-1}). The laser power was fixed at 1 mW, to avoid possible degradation of the analysed sample, while the adopted 50x objective yielded an illuminated area of about 2 μ diameter. To guarantee the measurement statistical reliability, the acquisition was repeated at 10x10 equally spaced points of a 25x25 μ^2 area. The average spectrum was, thus, calculated. On the other hand, the apparatus used for HPLC was a Jasco HPLC system (USA), consisting of a PU-2089 model intelligent solvent delivery pump, an AS-2057 autosampler model with a 10-100 μl injection loop, a computerized system controller, and a MD-2018 UV-Vis diode array (200-600 nm) detector. The same chromatographic separation discussed in Chapter 3 was performed, considering TBA.HSO_4 solution (0.006 M)/acetonitrile (64/36 v/v) at pH 5.0 ± 0.1 as mobile phase. The mobile phase was eluted at a flow rate of 0.6 ml/min and the effluent was monitored at 230 nm for 24 min. Although the polythionate chain length can be highly variable, the characterization of the liquid phase reaction product revealed that tetrathionate, pentathionate and hexathionate are essentially formed. On the other hand, the solid phase mainly consists on elemental sulphur (sulphur concentration in the solid phase higher than 98%, as proved in our previous work (Spatolisano et al., 2021b)). For this reason, its total weight is considered as the elemental sulphur content in solution.

3. Kinetic modelling

3.1 Kinetic scheme

Wackenroder's reaction (Wackenroder, 1846) has been systematically studied and mechanisms for the formation of polythionates have been advanced, but most of them are contradicted by radiochemical and radio-chromatographic investigations. A detailed study of the Wackenroder reaction has been proposed by Volynskii (Volynskii, 1971a, b), together with an excellent review of the available literature. The kinetic scheme disclosed by Volynskii considers the formation of thiosulphurous acid firstly, which decomposes into sulphur and sulphossilic acid. Due to the irreversibility of the first reaction steps (4), (5) and (6), sulphur formation is detected. Polythionates production occurs in solution through the reaction of thiosulphuric acid and sulphurous acid with mono or polyatomic sulphur. These sulphur species are intended to be the oxidizing agents. The H_2S role in the Wackenroder reaction is to generate mono or diatomic sulphur through the reaction with SO_2.

$$SO_2 + H_2S \rightarrow H_2S_2O_2 \tag{4}$$

$$H_2S_2O_2 \rightarrow S(OH)_2 + S \tag{5}$$

$$S(OH)_2 + H_2S \rightarrow S_2 + 2H_2O \tag{6}$$

$$H_2O + SO_2 \xleftrightarrow{K_a} HSO_3^- + H^+ \tag{7}$$

$$S + HSO_3^- \xleftrightarrow{K_t} HS_2O_3^- \tag{8}$$

$$S_2 + S \xrightarrow{k_3} S_3 \tag{9}$$

$$S_3 + S \xrightarrow{k_4} S_4 \tag{10}$$

$$S_4 + S \xrightarrow{k_5} S_5 \tag{11}$$

$$S_5 + S \xrightarrow{k_6} S_6 \tag{12}$$

$$S_6 + S \xrightarrow{k_7} S_7 \tag{13}$$

$$S + 2HSO_3^- \xleftrightarrow{K_2} S_2O_6^{2-} + H_2S \tag{14}$$

$$S_2 + 2HSO_3^- \xleftrightarrow{K_{3b}} S_3O_6^{2-} + H_2S \tag{15}$$

$$S + HSO_3^- + HS_2O_3^- \xleftrightarrow{K_{3a}} S_3O_6^{2-} + H_2S \tag{16}$$

$$S + 2HS_2O_3^- \xleftrightarrow{K_{4a}} S_4O_6^{2-} + H_2S \tag{17}$$

$$S_2 + HSO_3^- + HS_2O_3^- \xleftrightarrow{K_{4b}} S_4O_6^{2-} + H_2S \tag{18}$$

$$S_3 + 2HSO_3^- \xleftrightarrow{K_{4c}} S_4O_6^{2-} + H_2S \tag{19}$$

$$S_2 + 2HS_2O_3^- \xleftrightarrow{K_{5a}} S_5O_6^{2-} + H_2S \tag{20}$$

$$S_3 + HSO_3^- + HS_2O_3^- \xleftrightarrow{K_{5b}} S_5O_6^{2-} + H_2S \tag{21}$$

$$S_4 + 2HSO_3^- \xleftrightarrow{K_{5c}} S_5O_6^{2-} + H_2S \tag{22}$$

$$S_4 + HSO_3^- + HS_2O_3^- \xleftrightarrow{K_{6a}} S_6O_6^{2-} + H_2S \tag{23}$$

$$S_3 + 2HS_2O_3^- \xleftrightarrow{K_{6b}} S_6O_6^{2-} + H_2S \tag{24}$$

$$S_5 + 2HSO_3^- \xleftrightarrow{K_{6c}} S_6O_6^{2-} + H_2S \tag{25}$$

Depending on the reaction operating conditions, the formation of one or more polythionates can occur.

The presented reaction mechanism is considered as the starting point to derive the process kinetic scheme. As it is the series of many elemental steps, the following simplifications have been introduced to build up the detailed kinetic scheme:

- H_2SO_3 formation is assumed as negligible in the reaction zone, taking into account that the sulphurous acid formation already occurs in the absorption step. H_2SO_3 species is replaced with SO_2 and H_2O;
- $H_2S_2O_3$ formation is considered as negligible in the reaction zone. $H_2S_2O_3$ is replaced with S + SO_2 + H_2O;
- sulphur formation is described through (26), intended as the sum of reactions (4), (5) and (6) .

Following these hypotheses, two different alternatives have been considered for the derivation of the most suitable Wackenroder reaction kinetic scheme: the single-lump and two-lumps kinetic scheme (Pellegrini et al., 2004). According to the single-lump kinetic scheme, all the polythionates produced can be represented as one single ion species, the tetrathionate. The single lump kinetic scheme can be described through reactions (26) and (27).

$$2H_2S + SO_2 \rightarrow 3S + 2H_2O \tag{26}$$

$$3S + 2SO_2 + 2H_2O \xleftrightarrow{K_{4a}} S_4O_6^{2-} + 2H^+ + H_2S \tag{27}$$

$$4S + 2SO_2 + 2H_2O \xleftrightarrow{K_{5a}} S_5O_6^{2-} + 2H^+ + H_2S \tag{28}$$

In this case, all the polythionates are approximated as equivalent tetrathionate, as:

$$\left[mol\ S_4O_6^{2-,EQ}\right] = \left[mol\ S_4O_6^{2-}\right] + \frac{5}{4}\left[\frac{mol\ S_4O_6^{2-}}{mol\ S_5O_6^{2-}}\right]\cdot\left[mol\ S_5O_6^{2-}\right] + \frac{6}{4}\left[\frac{mol\ S_4O_6^{2-}}{mol\ S_6O_6^{2-}}\right]\cdot\left[mol\ S_6O_6^{2-}\right] \tag{29}$$

On the other hand, in the two-lumps kinetic scheme, all the polythionates produced are described through two representative classes: the tetrathionate and pentathionate (see reaction (28), together with reaction (27)). In the case of the two-lumps kinetic scheme, the hexathionate is approximated to equivalent pentathionate, evaluated as:

$$\left[mol\ S_5O_6^{2-,EQ}\right] = \left[mol\ S_5O_6^{2-}\right] + \frac{6}{5}\left[\frac{mol\ S_5O_6^{2-}}{mol\ S_6O_6^{2-}}\right]\cdot\left[mol\ S_6O_6^{2-}\right] \tag{30}$$

4. Kinetic parameters determination

As described in section 2, the reacting system considered is a gas-liquid one. H_2S, fed to the reactor in the gas – phase, has to diffuse into the liquid phase to be contacted with SO_2 liquid mixture, so that the liquid phase reaction can occur. Before starting to model the reacting system, it is necessary to:

- evaluate the mass-transfer and reacting phenomena rates, to determine the controlling regime, if any;
- identify the most suitable model to represent the experimental apparatus.

These points are discussed in section 4.1 and 4.2, respectively.

4.1 Identification of the controlling regime

The controlling regime has been identified through a qualitative analysis of the available experimental data, considering the system behaviour as a function of the operating conditions residence time, temperature and pressure. As suggested by Rose (Rose, 1981), mass-transfer controlled reaction rate is directly proportional to the mass-transfer area and independent of the liquid volume (as long as the same surface area is present). Also, the reaction is not highly temperature dependent, its rate being no more than directly proportional to temperature. On the other hand, the effect of pressure is more important on the gas-liquid mass-transfer phenomena than on the liquid kinetic ones. As for temperature, the mass-transfer phenomena are assumed to be not highly influenced by residence time (Astarita, 1967; Danckwerts, 1970).

Referring to the HydroClaus system, at the end of each test, both gas and liquid phase H_2S and SO_2 residual concentrations were measured through an in – line gas chromatograph. Since the reaction occurs in the liquid phase, the outlet H_2S gas phase flow rate depends on the diffusion rate of the component itself. If the kinetic regime is the controlling one, the mass-transfer phenomena are assumed to be fast and the H_2S gas phase flow rate does not vary in a significant way as a function of pressure. On the contrary, the outlet H_2S flow rate in the liquid phase is a function of the reaction kinetics. If the kinetic regime is the controlling one, the H_2S concentration in the liquid phase has to vary significantly with temperature and residence time. Starting from these evidences, Figure 2 shows the qualitative effect of the operating conditions on the outlet H_2S flow rates, both in the liquid and gas phases. Considering that the outlet H_2S gas phase flow rate is not variable with pressure, temperature and residence time, while the liquid phase H_2S outlet flow rates are highly influenced by temperature and residence time, the mass-transfer control has been excluded for this case and a kinetic regime has been assumed. To farther validate this hypothesis, the $\%H_2S$ transferred from the gas phase to the liquid phase and the $\%SO_2$ not transferred from the liquid phase to gas phase have been calculated for each experimental tests according to equations (31) and (32).

$$G \rightarrow L \qquad \%\mathrm{H_2S}^{transferred} = \left(\frac{F_{H_2S,G}{}^{IN} - F_{H_2S,G}{}^{OUT}}{F_{H_2S,G}{}^{IN}} \right) \cdot 100 \tag{31}$$

$$L \rightarrow G \qquad \%\mathrm{SO_2}^{not\ trasferred} = \left(\frac{F_{SO_2,L}{}^{IN} - F_{SO_2,G}{}^{OUT}}{F_{SO_2,L}{}^{IN}} \right) \cdot 100 \tag{32}$$

Since these quantities are close to 100% for each test, mass-transfer phenomena are assumed to be fast and the rate determining step of this system is the liquid phase reaction, which influences the rate of the entire process.

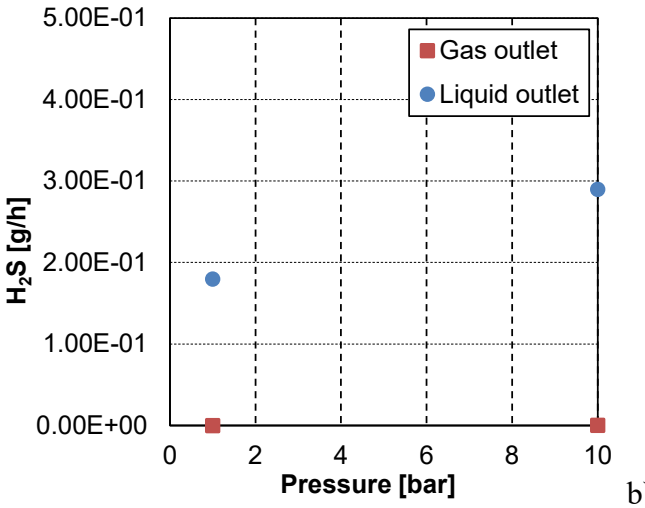

a)

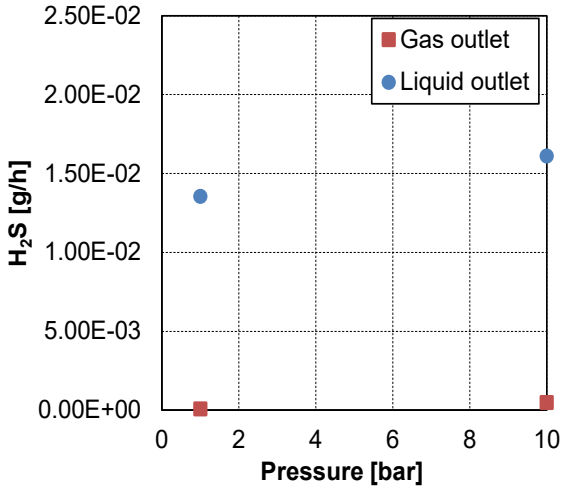

b)

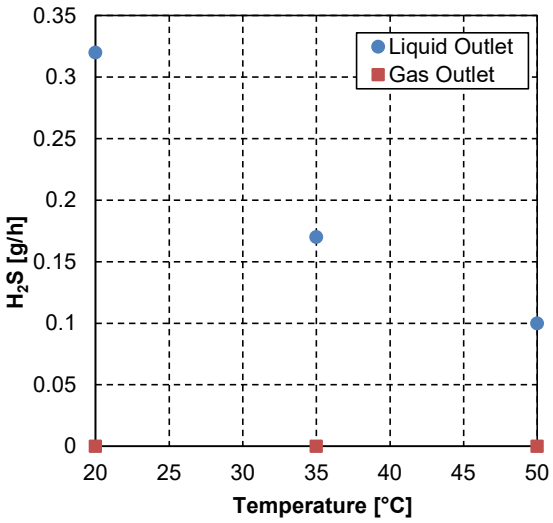

c)

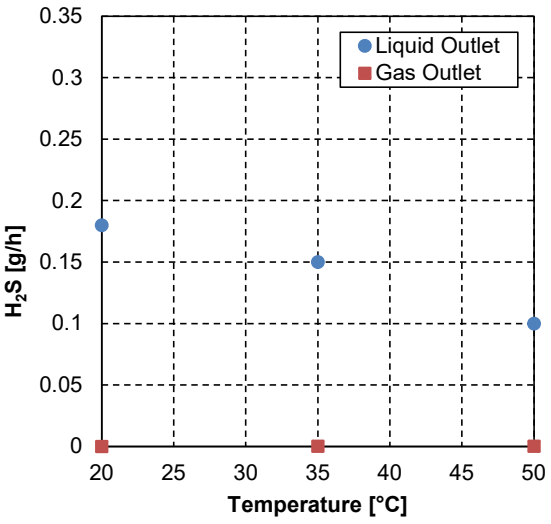

d)

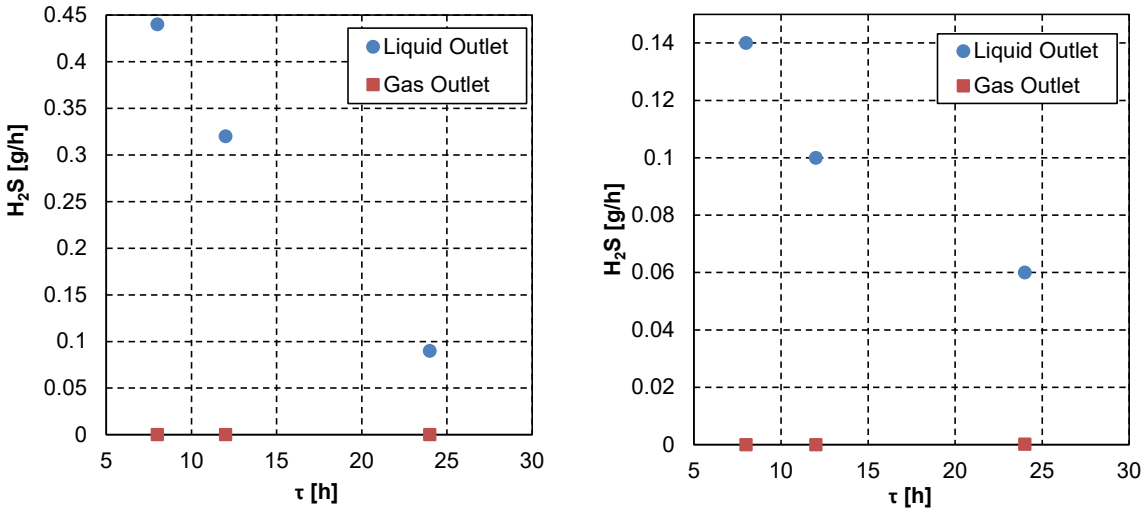

e) f)

Figure 2. Qualitative effect of the operating conditions on the H_2S outlet flow rates, considering: a) and b) pressure; c) and d) temperature; e) and f) residence time. The selected operating conditions are: a) T=20°C, V=2 l, H_2S^{IN}/SO_2^{IN}=0.462; b) T=20°C, V=2 l, H_2S^{IN}/SO_2^{IN}=1.847; c) P=3 bar, V=2.4 l, H_2S^{IN}/SO_2^{IN}=0.462; d) P=3 bar, V=2 l, H_2S^{IN}/SO_2^{IN}=0.462; e) T=20°C, P=3 bar, V=2.4 l; f) T=50°C, P=3 bar, V=2.4 l.

4.2 Reactor behaviour assessment

Actual reactors often perform in such a way that results lie between those predicted for tubular and continuous stirred tank reactors. In many continuous stirred tank reactors, the inlet and outlet pipes are close together. In this case, short circuiting can occur, so the reactor is modelled as perfectly mixed tank with a bypass stream (Cholette et al., 1960). In addition to short circuiting, stagnant regions (dead zones) are often encountered. In these regions there is no exchange of material with the well-mixed regions. Consequently, no reaction occurs there (Cholette and Cloutier, 1959).

Experiments have been carried out to determine the amount of the material effectively bypassed and the volume of the dead zone. The Residence Time Distribution (RTD) has been evaluated experimentally by injecting an inert chemical, called a tracer, into the reactor at time $t = 0$ and then measuring its concentration, C_{OUT}, in the effluent stream as a function of time. The tracer species has to be nonreactive, easily detectable and with physical properties similar to those of the reacting mixture. Thus, ethanol (EtOH) has been selected as tracer, also for its non-volatile behaviour at the operating temperature and pressure. A step tracer experiment (Figure 3) has been performed perturbing the system with 300 cc/h of ethanol aqueous solution at 3 wt.% at time $t = 0$. Since the value of the flow rate does not affect the results, 300 cc/h were fed for the sake of experimental convenience. In this way, each test lasted one day without completely filling the product storage tank. Four different tests have been considered, to analyse the system behaviour at variable impeller speeds. Results for these tests are reported in Figure 4 in terms of outlet tracer concentration as a function of time.

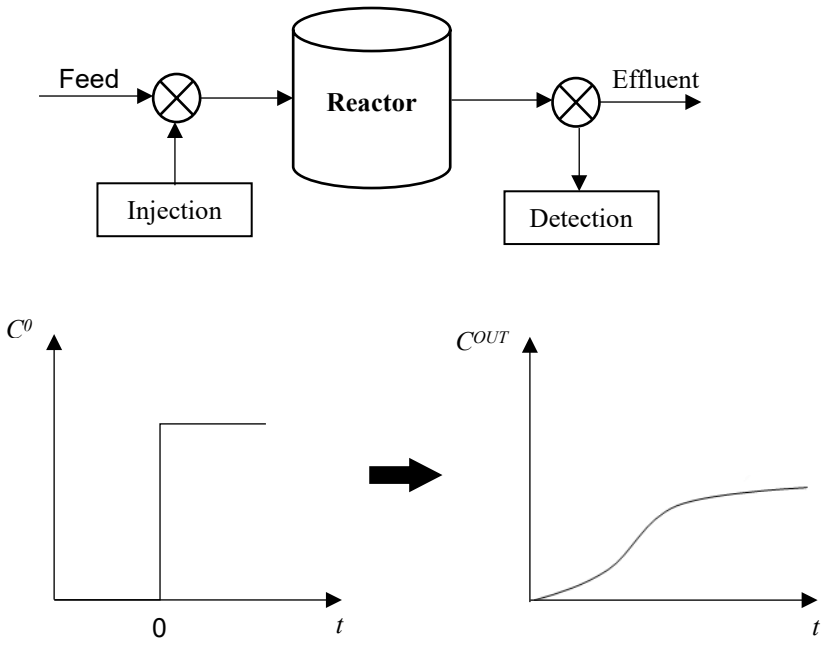

Figure 3. Schematization of the step tracer experiment for measuring the Residence Time Distribution (RTD) function (Fogler, 2016).

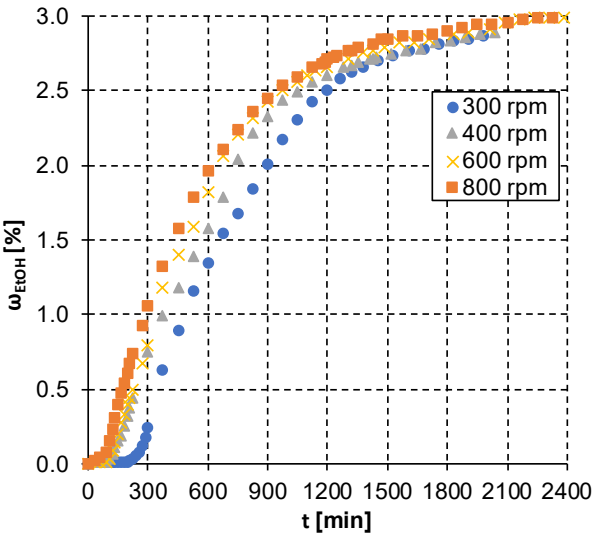

Figure 4. EtOH mass fraction (ω_{EtOH}) as a function of time t at various impeller speeds.

From Figure 4 a time delay is visible, particularly for the lowest value of the impeller speed (300 rpm), that disappears at higher impeller speeds (800 rpm). This time delay suggests that the reactor can be modelled as one PFR – CSTR series, probably because of too long inlet and outlet pipes (Levenspiel, 1999).

The residence time distribution function and cumulative time distribution functions have been evaluated according to equations (33) and (34). They are reported, for each test performed, in Figure 5 and Figure 6.

$$F(t) = \left[\frac{C_{OUT}}{C_0} \right]_{STEP} \tag{33}$$

$$E(t) = \frac{d}{dt} F(t) \tag{34}$$

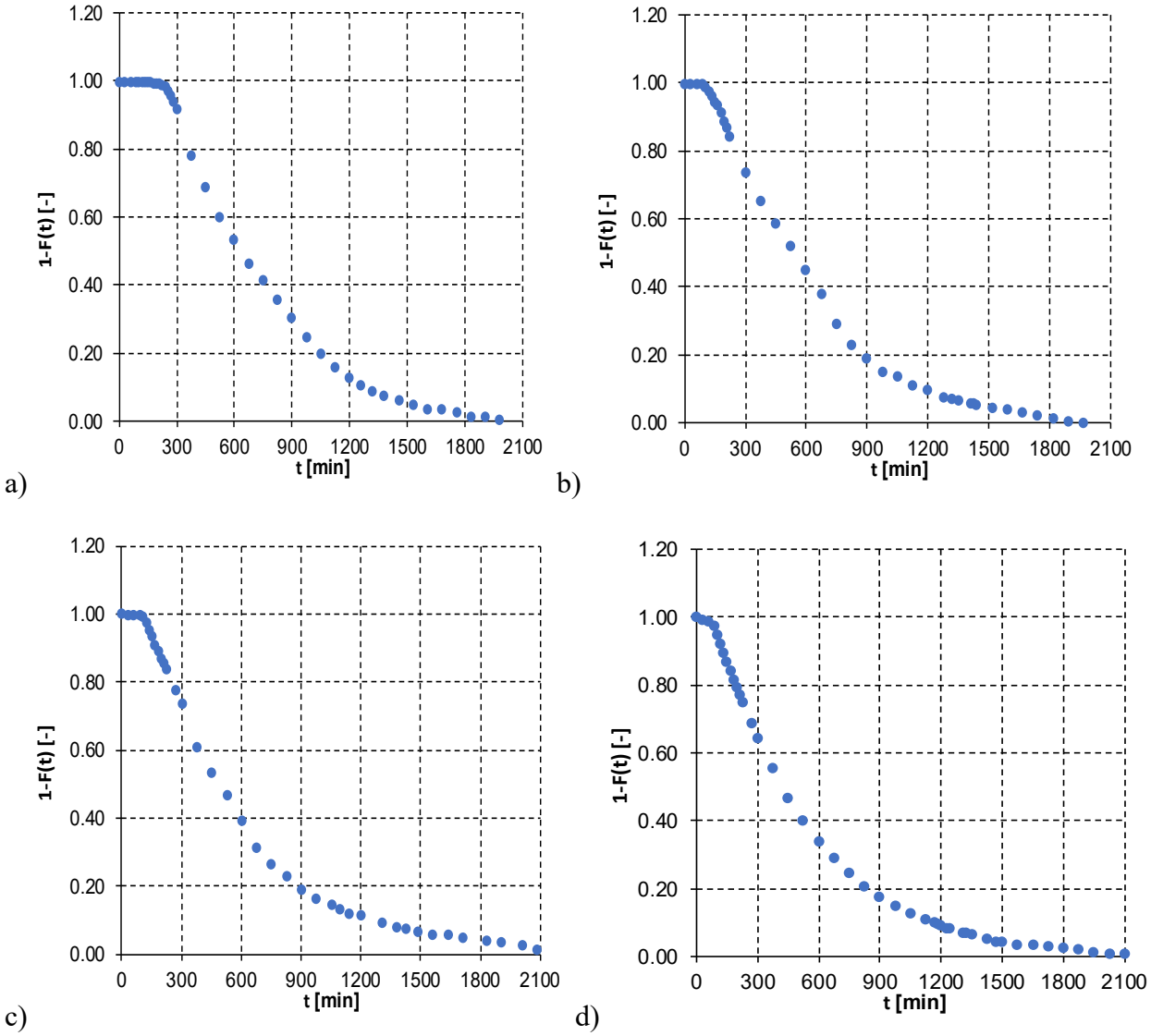

Figure 5. *Cumulative distribution function* (*F(t)*) for the case: a) 1 (v_{agit} = 300 rpm); b) 2 (v_{agit} = 400 rpm); c) 3 (v_{agit} = 600 rpm); d) 4 (v_{agit} = 800 rpm).

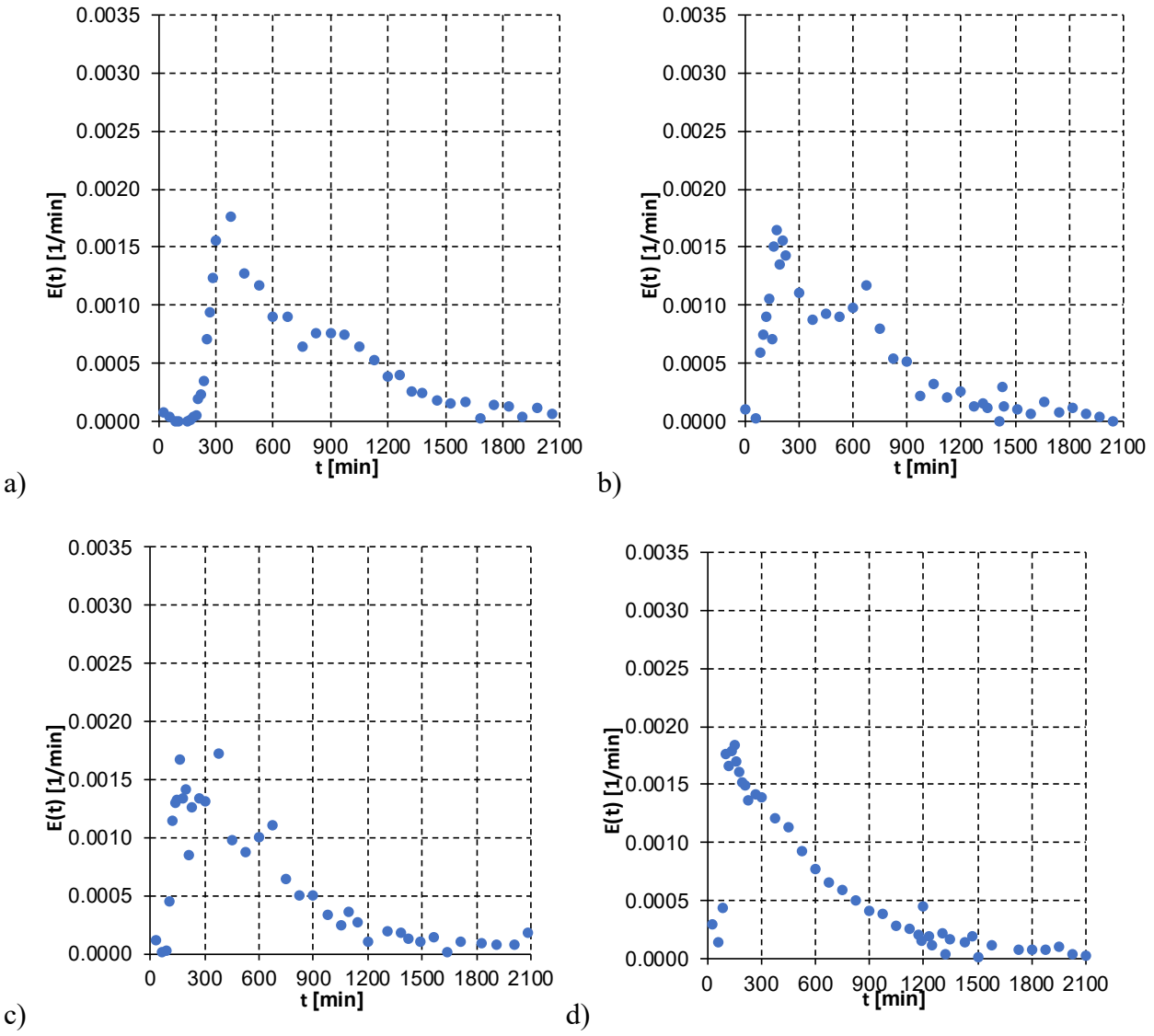

Figure 6. *Residence Time Distribution function* (*E(t)*) for the case: a) 1 (v_{agit} = 300 rpm); b) 2 (v_{agit} = 400 rpm); c) 3 (v_{agit} = 600 rpm); d) 4 (v_{agit} = 800 rpm).

The comparison between Figure 5 and Figure 6 curves with the reactor compartment flow models available in literature reveals the absence of a bypass. The cumulative distribution functions and RTD distribution functions confirm the PFR-CSTR series behaviour. This departure from ideal conditions tends to disappear at higher impeller speed. At v_{agit} = 800 rpm, the reactor behaviour seems to be ideal. The non idealities (i.e., dead volumes or bypass) of the stirred reactor have been quantified as suggested by Fogler (Fogler, 2016). To evaluate them, the experimental apparatus has been schematized as in Figure 7, being α the effective reactor volume fraction and λ the fraction of liquid flowed that bypasses the reaction zone. Assuming the reactor as control volume, a balance on the EtOH species is performed, considering that ethanol is inert.

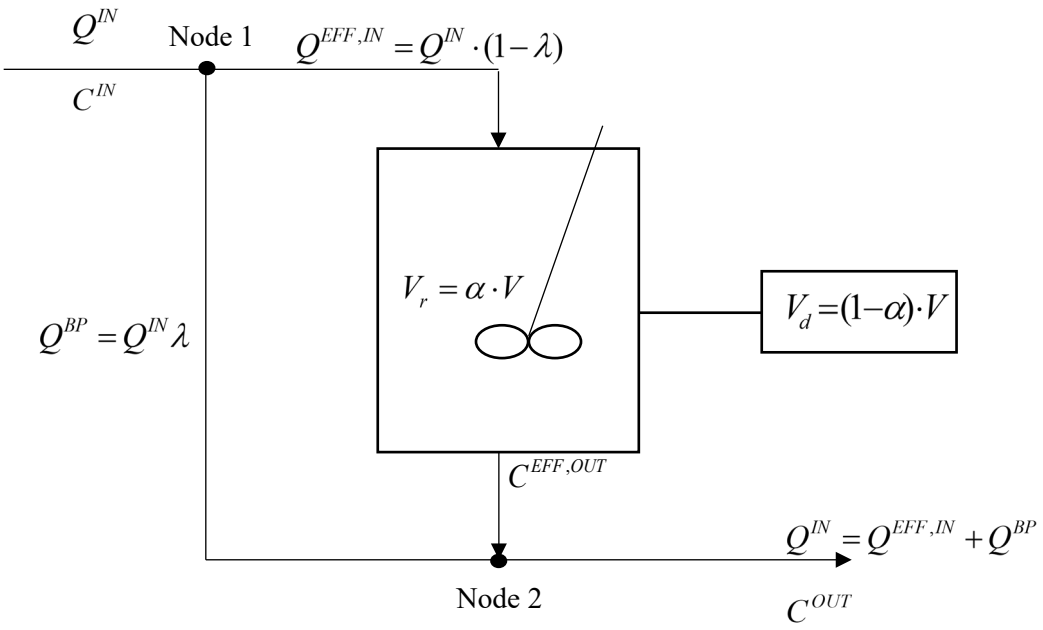

Figure 7. Schematization of the stirred tank reactor to quantify bypass and dead volumes.

$$V_r \frac{dC^{EFF,OUT}}{dt} = Q^{EFF,IN} \cdot C^{IN} - Q^{EFF,IN} \cdot C^{EFF,OUT} \tag{35}$$

$$Q^{EFF,IN} = Q^{IN} \cdot (1-\lambda) \tag{36}$$

$$Q^{BP} = Q^{IN} \lambda \tag{37}$$

$$Q^{EFF,IN} = Q^{IN} \cdot (1-\lambda) \tag{38}$$

$$\tau = \frac{V}{Q^{IN}} \tag{39}$$

Equation (35) integration leads to equation (40). Through an EtOH balance around Node 2 in Figure 7, the tracer concentration in the effluent stream results from equation (41). Ethanol balance can be thus written as equation (42) or equation (43).

$$\frac{C^{EFF,OUT}}{C^{IN}} = 1 - \exp\left[-\frac{1-\lambda}{\alpha}\left(\frac{t}{\tau}\right)\right] \tag{40}$$

$$C^{OUT} = \frac{Q^{BP} \cdot C^{IN} + Q^{EFF,IN} \cdot C^{EFF,OUT}}{Q^{IN}} \tag{41}$$

$$\frac{C^{OUT}}{C^{IN}} = 1 - (1-\lambda)\exp\left[-\frac{1-\lambda}{\alpha}\left(\frac{t}{\tau}\right)\right] \tag{42}$$

$$\ln\left(\frac{C^{IN}}{C^{IN} - C^{OUT}}\right) = \ln\left(\frac{1}{1-\lambda}\right) + \left[\frac{1-\lambda}{\alpha}\left(\frac{t}{\tau}\right)\right] \tag{43}$$

Therefore, considering a semilogarithmic plane with time on x axis and the concentration ratio on y axis, a line is obtained with slope $\left[\frac{1-\lambda}{\alpha}\left(\frac{1}{\tau}\right)\right]$ and intercept $\ln\left(\frac{1}{1-\lambda}\right)$. The slope and intercept of this line allows the quantification of both bypass and dead volumes.

Figure 8 reports the concentration ratio as a function of time for all the step tracer experiments performed.

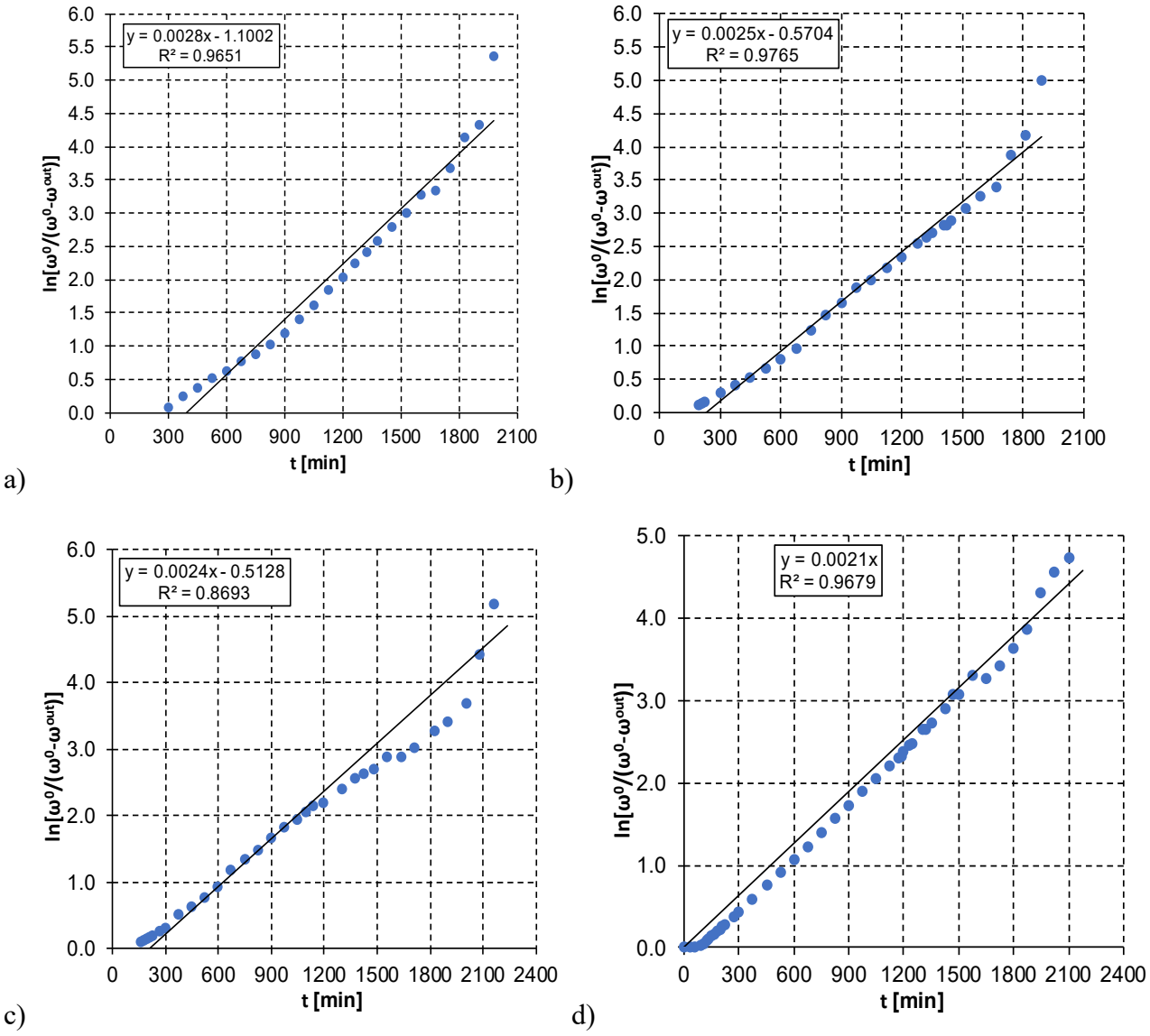

Figure 8. Representation of the concentration ratio as a function of time (t) on a semi-logarithmic scale for the test: a) 1 (v_{agit} = 300 rpm); b) 2 (v_{agit} = 400 rpm); c) 3 (v_{agit} = 600 rpm); d) 4 (v_{agit} = 800 rpm).

As can be seen in Figure 8, no bypass is present, since no positive intercept is available, but a dead volume is visible which disappears at v_{agit} = 800 rpm. Table 1 reports the evaluated effective volume for each test performed. Consequently, v_{agit} = 900 rpm has been selected as the impeller speed for performing experimental tests, to ensure an ideal behaviour for the reactor.

Table 1. Fraction of effective volume for all the tracer experiments performed at variable v_{agit}.

v_{agit} [rpm]	α [-]
300	0.74
400	0.83
600	0.87
800	0.99

4.3 Reactor modelling

As the reactor behaviour is ideal and the kinetic regime is the controlling one, the experimental apparatus can be represented as a CSTR with a single liquid phase (see Figure 9). Thereby, it can be modelled according to (44) for the single lump kinetic scheme and to (45) for the two-lumps kinetic scheme.

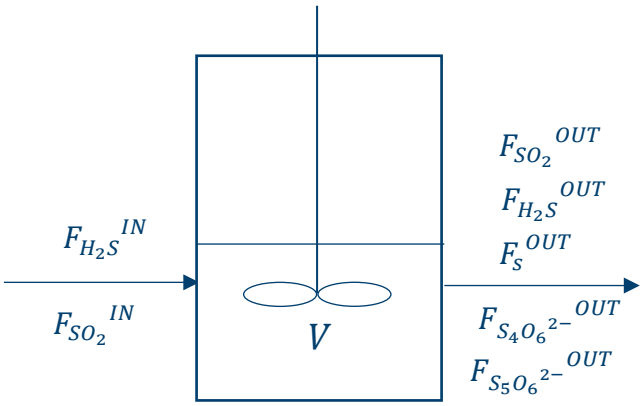

Figure 9. Experimental apparatus representation as a CSTR made by a single liquid phase.

$$\begin{cases} C_{H_2S}{}^{IN} - C_{H_2S}{}^{OUT} + \left(-2r_S + r_{S_4}\right)\cdot\tau = 0 \\ C_{SO_2}{}^{IN} - C_{SO_2}{}^{OUT} - \left(r_S + 2r_{S_4}\right)\cdot\tau = 0 \\ -C_{S_4O_6{}^{2-}}{}^{OUT} + r_{S_4}\cdot\tau = 0 \\ -C_S{}^{OUT} + 3\left(r_S - r_{S_4}\right)\cdot\tau = 0 \end{cases} \tag{44}$$

$$\begin{cases} C_{H_2S}{}^{IN} - C_{H_2S}{}^{OUT} + \left(-2r_S + r_{S_4} + r_{S_5}\right)\cdot\tau = 0 \\ C_{SO_2}{}^{IN} - C_{SO_2}{}^{OUT} - \left(r_S + 2r_{S_4} + 2r_{S_5}\right)\cdot\tau = 0 \\ -C_{S_4O_6^{2-}}{}^{OUT} + r_{S_4}\cdot\tau = 0 \\ -C_{S_5O_6^{2-}}{}^{OUT} + r_{S_5}\cdot\tau = 0 \\ -C_S{}^{OUT} + \left(3r_S - 3r_{S_4} - 4r_{S_5}\right)\cdot\tau = 0 \end{cases} \tag{45}$$

The reaction rates expressions which appear in (44) and (45) are detailed in equations (46) to (48). In these expressions, A is the pre-exponential factor, E_{ATT} is the activation energy, while the concentration exponents α, β, γ, δ, ε, θ are the reaction orders.

$$r_S = A_S \cdot \exp\left(\frac{-E_{ATT,S}}{RT}\right)\cdot\left(C_{H_2S}\right)^{\alpha}\cdot\left(C_{SO_2}\right)^{\beta} \tag{46}$$

$$r_{S_4} = \overrightarrow{A_4}\cdot\exp\left(\frac{-\overrightarrow{E}_{ATT,4}}{RT}\right)\cdot\left(C_S\right)^{\gamma}\cdot\left(C_{SO_2}\right)^{\delta} - \overleftarrow{A_4}\cdot\exp\left(\frac{-\overleftarrow{E}_{ATT,4}}{RT}\right)\cdot\left(C_{H_2S}\right)^{\varepsilon}\cdot\left(C_{S_4O_6^{2-}}\right)^{\vartheta} \tag{47}$$

$$r_{S_5} = \overrightarrow{A_5}\cdot\exp\left(\frac{-\overrightarrow{E}_{ATT,5}}{RT}\right)\cdot\left(C_S\right)^{\gamma}\cdot\left(C_{SO_2}\right)^{\delta} - \overleftarrow{A_5}\cdot\exp\left(\frac{-\overleftarrow{E}_{ATT,5}}{RT}\right)\cdot\left(C_{H_2S}\right)^{\varepsilon}\cdot\left(C_{S_4O_6^{2-}}\right)^{\vartheta} \tag{48}$$

The species experimental concentrations are evaluated starting from the experimental data according to equations (49) to (53).

$$C_{H_2S} = \frac{F_{H_2S}{}^{OUT}}{Q_L}\ \left[mol/l\right] \tag{49}$$

$$C_{SO_2} = \frac{F_{SO_2}{}^{OUT}}{Q_L}\ \left[mol/l\right] \tag{50}$$

$$C_S = \frac{F_S{}^{OUT}}{Q_L{}^{OUT}}\ \left[mol/l\right] \tag{51}$$

$$C_{S_4O_6^{2-}} = \frac{F_{S_4O_6^{2-}}{}^{OUT}}{Q_L{}^{OUT}}\ \left[mol/l\right] \tag{52}$$

$$C_{S_5O_6^{2-}} = \frac{F_{S_5O_6^{2-}}{}^{OUT}}{Q_L{}^{OUT}}\ \left[mol/l\right] \tag{53}$$

The parameters which appear in the kinetic expressions (i.e., pre-exponential factor, activation energies and reaction orders) are evaluated through a non-linear regression routine in 5 variables (T,

C_{H_2S}, C_{SO_2}, C_S, $C_{S_4O_6^{2-}}$), in the case of the single lump kinetic scheme, or 6 variables, in the case of the two-lumps kinetic scheme (T, C_{H_2S}, C_{SO_2}, C_S, $C_{S_4O_6^{2-}}$, $C_{S_5O_6^{2-}}$).

An ad-hoc developed FORTRAN routine allows determining the value of parameters which minimizes the difference between the experimental and calculated reaction rates, (Froment et al., 2010), thanks to the minimum square method.

5. Results and discussion

5.1 Single lump kinetic scheme

In the case of the single-lump kinetic scheme, the evaluated kinetic parameters are reported in Table 2 and Table 3, together with the calculated coefficient of determination R^2. The unit of measurement of pre-exponential factors can be determined considering that the reaction rates are expressed in [mol/(l·h)], while concentrations and time are measured in [mol/l] and [h], respectively.

Table 2. Reaction (46) parameters values for the single lump kinetic scheme.

parameter	value
A_S	76.7689
$E_{ATT,S}$ [J/mol]	1.8528E+04
α	0.20
β	-0.26
R^2	0.92

Table 3. Reaction (47) parameters values for the single lump kinetic scheme.

parameter	value
$\vec{A}_4$	10.8576
$\vec{E}_{att,4}$[J/mol]	1.8140E+04
Υ	-0.40
δ	-0.05
$\overleftarrow{A}_4$	5.7036E+15
$\overleftarrow{E}_{att,4}$	9.7145E+04

ε	11.49
θ	-14.62
R^2	0.92

To verify the model reliability, model predictions have been compared with the available experimental data. They are reported in terms of reactants conversions (Figure 10) and products concentrations (Figure 11) as a function of time.

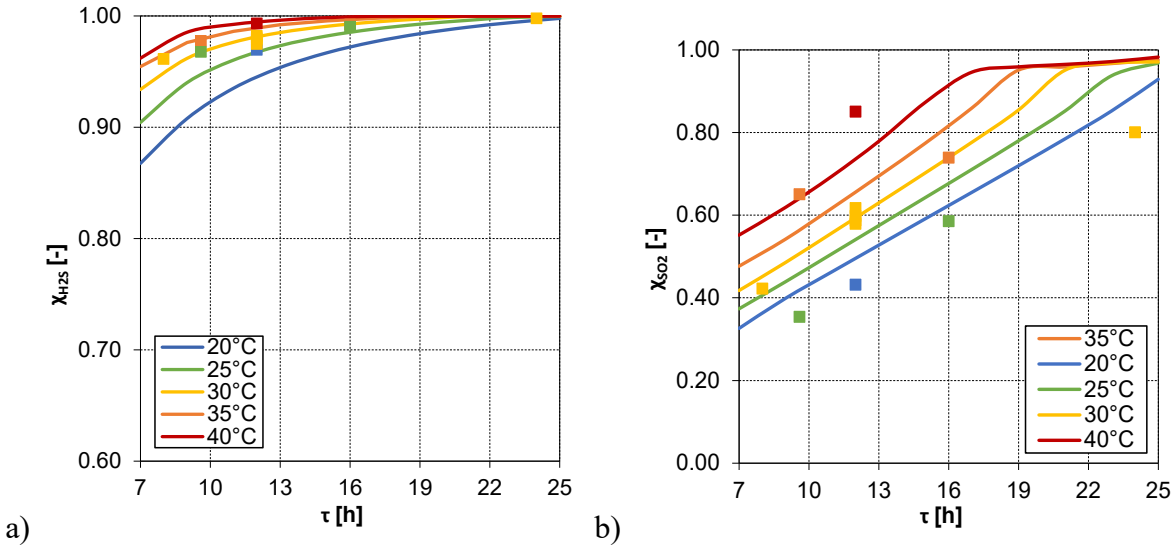

Figure 10. Reactants conversion as a function of residence time (τ) and at variable T for: a) H_2S, b) SO_2, considering the single lump kinetic scheme.

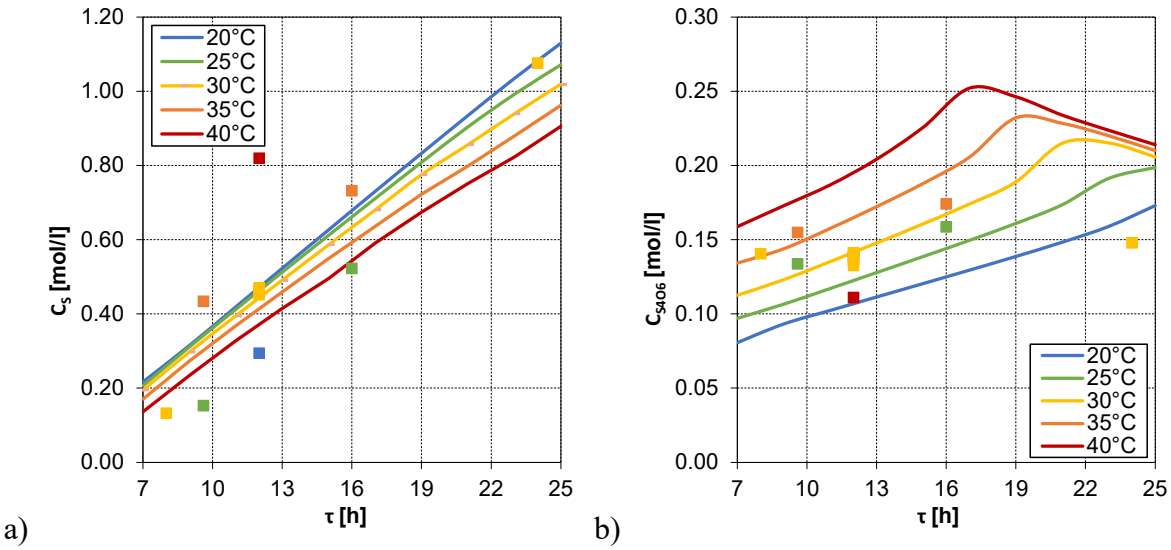

Figure 11. Concentration as a function of residence time (τ) and at variable temperature T for: a) S, b) S_4O_6, considering the single lump kinetic scheme.

Model predictions show a not satisfactory agreement with the experimental points, particularly as regards the sulphur and tetrathionate concentrations. Specifically, the sulphur concentration model predictions show an opposite trend as a function of temperature if compared to that of the experimental data. Therefore, it's possible to conclude that tetrathionate alone is not able to describe the system kinetics. The calculation of the equivalent tetrathionate, in fact, causes the superposition of two different behaviours: the $S_4O_6^{2-}$ one, on the one hand, and the $S_5O_6^{2-}$ and $S_6O_6^{2-}$ones, on the other hand, reported in Figure 12 for the sake of clarity.

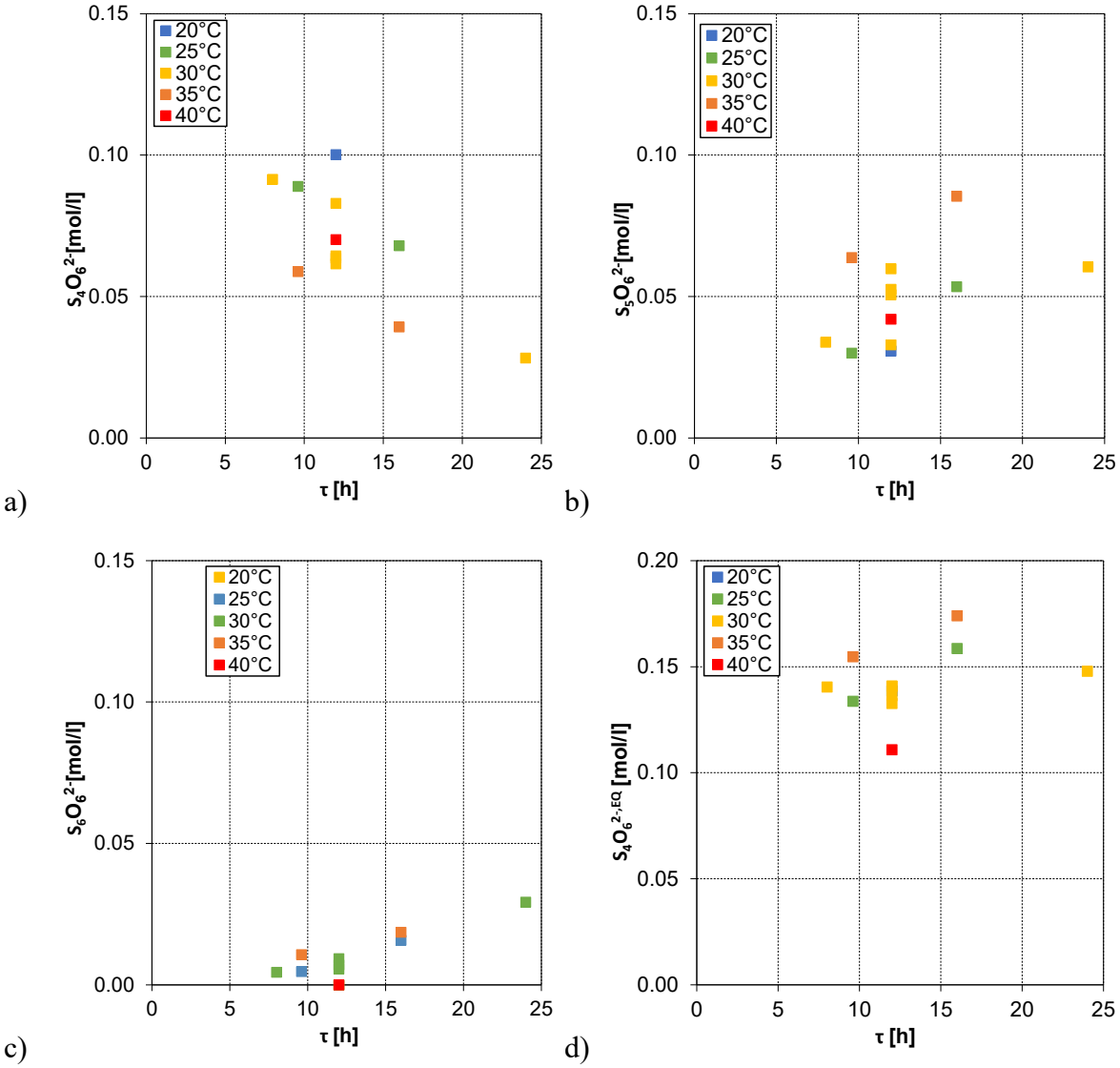

Figure 12. Concentration of: a) $S_4O_6^{2-}$ ($S_4O_6^{2-}$); b) $S_5O_6^{2-}$ ($S_5O_6^{2-}$); b) $S_6O_6^{2-}$ ($S_6O_6^{2-}$) and d) $S_4O_6^{2-,EQ}$ ($S_4O_6^{2-,EQ}$) as a function of residence time (τ) and at variable temperature *T*.

As shown in Figure 12, the pentathionate and hexathionate concentrations are monotonically increasing with τ and T (except for the experimental point at T = 40° C). The opposite is for the tetrathionate, whose concentration decreases with τ and T. Globally, tetrathionate is the most abundant species at low residence times; as τ increases, pentathionate is preponderant. This evidence

seems, at first glance, to be in contrast with what expected: as the temperature and residence time increase, the polythionates concentration in the process should decrease in favour of sulphur production. The only likely explanation to justify the observed trend is that the measured pentathionate and hexathionate concentrations are the result of disproportionation/decomposition processes of the longer homologues, not detected by the current characterization technique. Furthermore, since the hexathionate concentration is very low, this measurement is significantly affected by the Limit Of Quantification (LOQ) of the instrument.
As a result, the two-lump kinetic scheme is considered, introducing the pentathionate.

5.2 Two-lumps kinetic scheme

Regarding the two-lumps kinetic scheme, Table 4, Table 5 and Table 6 summarize the value of the regressed kinetic parameters. In these tables, the unit of measurement of pre-exponential factors can be determined considering that the reaction rates are expressed in [mol/(l·h)], while concentrations and time are measured in [mol/l] and [h], respectively.

Table 4. Reaction (46) parameters values for the two-lumps kinetic scheme.

parameter	value
A_S	21.4946
$E_{ATT,S}$ [J/mol]	1.5294E+04
α	0.21
β	-0.29
R^2	0.92

Table 5. Reaction (47) parameters values for the two-lumps kinetic scheme.

parameter	value
$\vec{A}_4$	20.1635
$\vec{E}_{att,4}$ [J/mol]	1.7899E+04
Υ	-0.15
δ	1.29
$\overleftarrow{A}_4$	6.0417E+14

$\overleftarrow{E}_{att,4}$	1.5685E+05
ε	11.94
θ	-14.98
R^2	0.95

Table 6. Reaction (48) parameters values for the two-lumps kinetic scheme.

parameter	value
$\vec{A}_5$	370.4030
$\vec{E}_{att,5}$[J/mol]	2.8137E+04
Υ	-0.20
δ	0.13
$\overleftarrow{A}_5$	6.9072E+12
$\overleftarrow{E}_{att,5}$	8.1679E+04
ε	2.39
θ	-2.36
R^2	0.89

Model predictions and their relative comparison with the experimental points are reported in Figure 13, in terms of reactants conversions and Figure 14, in terms of products concentrations.

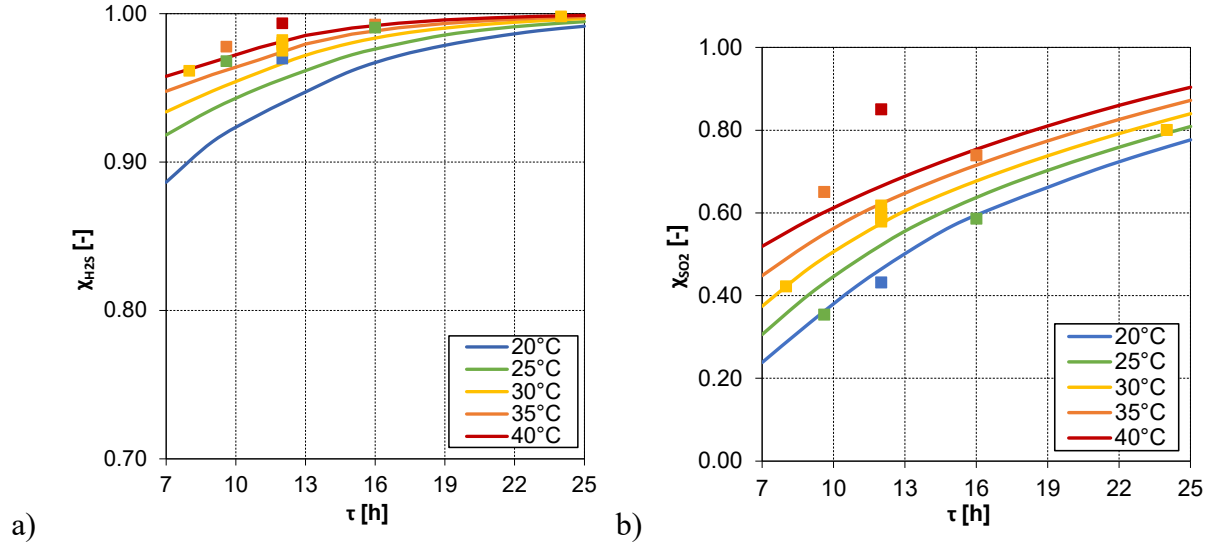

Figure 13. Reactants conversion as a function of residence time (τ) and at variable T for: a) H_2S, b) SO_2, considering the two-lumps kinetic scheme. Comparison between model (solid lines) and experimental data (squares).

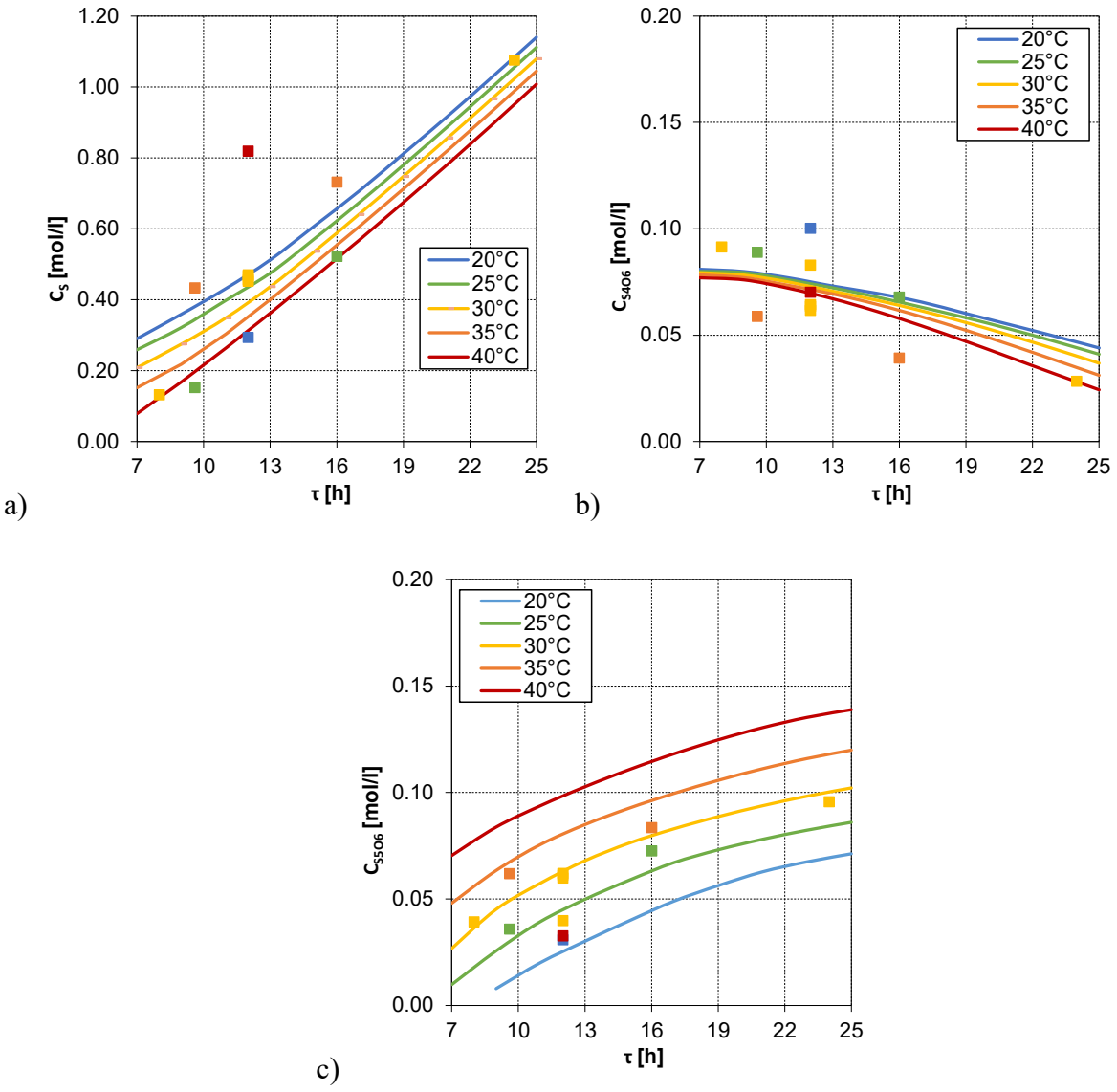

Figure 14. Concentration as a function of residence time (τ) and at variable temperature T for: a) S, b) S_4O_6, c) S_4O_6 considering the two-lumps kinetic scheme. Comparison between model (solid lines) and experimental data (squares).

The agreement between the model and the experimental data, in the case of the two-lumps kinetic scheme, is satisfactory as regards the reactants conversion and the pentathionate concentration. Still, a deviation between model and experimental data is observed for both sulphur and tetrathionate concentration.

Following the Volynskii reaction mechanism, sulphur results from a complex series of reactions, that probably the simplified kinetic scheme cannot completely fit. The observed experimental data trend can be motivated considering the decomposition/disproportionation reactions of higher homologues into lower one, for instance:

$$S_5O_6^{2-} \rightarrow S + S_4O_6^{2-} \tag{54}$$

that take place at high temperature, particularly. As a matter of fact, at $T = 40°C$, none of the discussed models can accurately predict the experimental observations, according to which a higher $S_4O_6{}^{2-}$ and a lower $S_5O_6{}^{2-}$ concentration is detected. At this stage, considering the available experimental data (12 points), a more detailed kinetic scheme cannot be reasonably faced.

6. Conclusion

In this work, the HydroClaus kinetics, a novel H_2S valorization process patented by Eni S.p.A., has been analysed for the first time. A step tracer experiment has been performed for assessing the experimental apparatus behaviour, while a qualitative analysis of the available tests allows identifying the controlling regime, that was the kinetic regime. The kinetic phenomena involved in the process appear as very complex, considering both the high number of reactions involved and the product mixture nature. The kinetic schemes discussed pave the way for the reacting system comprehension, considering the available experimental points. All the analysed models have:

- same E_{att} order of magnitude;
- $\alpha > 0$ e $\beta < 0$: the sulphur reaction rate is higher at increasing $\frac{H_2S}{SO_2}$, as reported in literature;
- $\tilde{r}_{S_4}$ e $\tilde{r}_{S_5}$ reaction rates, responsible for tetrathionate and pentathionate decomposition, increase at increasing $\frac{H_2S}{S_4O_6{}^{2-}}$ e $\frac{H_2S}{S_5O_6{}^{2-}}$ ratios, respectively.

Among all the analysed models, the single lump kinetic scheme is the simplest. Nevertheless, it's not suitable to describe all the system's reacting phenomena: the introduced simplification is responsible for a complex superimposition of the effects. On the other hand, the two-lumps kinetic scheme seems more suitable to represent the system's kinetics. A further investigation with more experimental points is needed for a deeper clarification of the reacting system.

References

Astarita, G., 1967. Mass transfer with chemical reaction.

Barbieri, R., Croatto, U., 1964. Il meccanismo della reazione di Wackenroder. La ricerca scientifica, anno 34, rendiconti A 4.

Barbieri, R., Faraglia, G., 1962. Indagini sulla reazione di Wackenroder.- Nota II. Sul meccanismo di formazione dello zolfo interno degli acidi politionici. Gazzetta Chimica Italiana 92, 660 – 675.

Borsboom, J., Van Warners, A., Van Nisselrooij, P.F.M.T., Van Yperen, R., Chopra, V., 2005. Recovery of sulfur from a hydrogen sulfide containing gas.

Cholette, A., Banchet, J., Cloutier, L., 1960. Performance of Flow Reactors at Various Levels of Mixing. The Canadian Journal of chemical Engineering, 1-18.

Cholette, A., Cloutier, L., 1959. Mixing Efficiency Determinations for Continuous Flow Systems. The Canadian Journal of chemical Engineering, 105-112.

Danckwerts, P.V., 1970. Gas-Liquid Reactions.

de Angelis, A., Palazzina, M., Pollesel, P., Cobianco, S., Lockhart, T., 2005. Process for the production of sulphur starting from the hydrogen sulfide contained in the natural gas or in the associated gas and possible disposal of the thus obtained sulfur, in: S.p.A., E. (Ed.).

De Guido, G., Fogli, M.R., Pellegrini, L.A., 2018. Effect of Heavy Hydrocarbons on CO_2 Removal from Natural Gas by Low-Temperature Distillation. Industrial & engineering chemistry research 57, 7245-7256.

De Guido, G., Pellegrini, L.A., Besagni, G., Inzoli, F., 2017. Acid Gas Removal from Natural Gas by Water Washing. Chemical Engineering Transactions 57, 1129-1134.

Fogler, H.S., 2016. Elements of Chemical Reaction Engineering.

Froment, G.F., Bishoff, K.B., De Wilde, J., 2010. Chemical Reactor Analysis and Design, 3rd Edition ed.

Groenendaal, W., 1974. Process for reducin the total sulfur content of claus off-gases, in: Shell Oil Company, N.Y., N.Y. (Ed.).

Heinrich, G., Kasztelan, S., 2001. Hydrotreating. Petroleum Refining. Conversion Processes.

Kunkel, L.W., Palm, W.J., Petty, L.E., Grekel, H., 1977. CBA for claustail gas cleanup.

Levenspiel, O., 1999. Chemical Reaction Engineering, Third ed.

Pellegrini, L.A., De Guido, G., Valentina, V., 2019. Energy and exergy analysis of acid gas removal processes in the LNG production chain. Journal of Natural Gas Science and Engineering 61, 303-319.

Pellegrini, L.A., Locatelli, S., Rasella, S., Bonomi, S., Calemma, V., 2004. Modeling of Fischer–Tropsch products hydrocracking. Chemical Engineering Science 59, 4781-4787.

Rose, L.M., 1981. Chemical Reactor Design in Practice.

Rouquette, C., Digne, M., Renaudot, L., Grandjean, J., Ballaguet, J.P., 2009. Monitoring of the Chemical Species in a Liquid-Phase Claus Reaction. Energy Fuels 23, 4404–4412.

Spatolisano, E., de Angelis, A.R., Pellegrini, L.A., 2021a. Middle scale hydrogen sulphide conversion and valorization technologies: a review. Submitted to ChemBioEng Reviews.

Spatolisano, E., Pellegrini, L.A., Gelosa, S., Broglia, F., Bonoldi, L., de Angelis, A.R., Moscotti, D.G., Nali, M., 2021b. Polythionic acids in the Wackenroder reaction. ACS Omega 6, 26140-26149.

Volynskii, N.P., 1971a. Mechanism of Wackenroder Reaction. Russ. J. Inorg. Chem. 16, 158-161.

Volynskii, N.P., 1971b. Thiosulphuric acid. Polythionates. The Wackenroder reaction.

Wackenroder, H., 1846. Über eine neue Säure des Schwefels. Arch. Pharm. 97, 272-288.